Evaluation of cardiac findings using speckle-tracking echocardiography in fetuses with hemoglobin Bart's disease

S. ANUWUTNAVIN[1] , K. RUSSAMEECHAROEN[1], P. RUANGVUTILERT[1], S. VIBOONCHARD[1], C. YAIYIAM[1], M. SKLANSKY[2] and G. R. DEVORE[3,4]

[1]*Division of Maternal-Fetal Medicine, Department of Obstetrics and Gynecology, Faculty of Medicine, Siriraj Hospital, Mahidol University, Bangkok, Thailand;* [2]*Division of Pediatric Cardiology, Department of Pediatrics, UCLA Mattel Children's Hospital, David Geffen School of Medicine, UCLA, Los Angeles, CA, USA;* [3]*Division of Maternal-Fetal Medicine, Department of Obstetrics and Gynecology, David Geffen School of Medicine, UCLA, Los Angeles, CA, USA;* [4]*Fetal Diagnostic Centers, Pasadena, CA, USA*

CONTRIBUTION

What are the novel findings of this work?
Abnormal left global and longitudinal systolic contractility is already evident in the early stage of Bart's anemia during mid-gestation in non-hydropic fetuses. Combined fetal cardiac measurements derived from speckle-tracking analysis, as a function of head circumference, outperformed previously reported ultrasound measurements of the cardiothoracic ratio, middle cerebral artery peak systolic velocity and placental thickness in predicting the development of hemoglobin Bart's disease.

What are the clinical implications of this work?
Fetal cardiac measurements using speckle-tracking analysis may provide the capability to precisely detect early changes in the fetal heart during the second trimester in fetuses at risk for developing Bart's anemia. This technique has the potential to improve prenatal diagnostic accuracy and decrease false-positive rates compared with using previously reported sonographic markers. It may aid in early diagnosis and management before the onset of fetal hydrops.

ABSTRACT

Objective Hemoglobin (Hb) Bart's disease is a severe manifestation of alpha-thalassemia, resulting in fetal tissue hypoxia and severe anemia. There is limited research available on assessing speckle-tracking analysis of the fetal heart as a response to fetal anemia caused by Hb Bart's disease. This study aimed to assess the diagnostic performance of fetal cardiac measurements derived from speckle-tracking analysis to identify fetuses with Bart's anemia between 17 and 24 weeks of gestation.

Methods This prospective cohort study included 115 women with singleton pregnancies at risk for fetal Hb Bart's disease who underwent either amniocentesis or cordocentesis at Siriraj Hospital, Bangkok, Thailand, in the period between January 2019 and January 2021. Speckle-tracking analysis of the fetal heart was performed in the four-chamber view (4CV), assessing ventricular size and shape, ventricular contractility and left ventricular function, prior to invasive prenatal testing. Logistic regression analysis was used to determine significant cardiac predictors and calculate the probability of a fetus having Hb Bart's anemia.

Results Among the cohort, 38 (33.0%) fetuses were diagnosed with Hb Bart's disease, and of these, nine (23.7%) cases exhibited fetal hydrops. In comparison to the control group, affected fetuses displayed enlargement of the 4CV, with a globular shape of the right ventricular chamber. Additionally, there were significant reductions in both global and longitudinal left ventricular contractility in non-hydropic affected fetuses compared with the controls. At mid-gestation, no significant differences were observed in transverse contractility or left ventricular function, except for the ejection fraction, between the two groups. Based on logistic regression analysis, combined cardiac measurements derived from speckle-tracking analysis, as a function of head circumference, could differentiate non-hydropic

Correspondence: Dr S. Anuwutnavin, Department of Obstetrics and Gynecology, Faculty of Medicine, Siriraj Hospital, Mahidol University, 2 Prannok Road, Bangkoknoi, Bangkok 10700, Thailand (e-mail: asanitra@hotmail.com)

ORIGINAL PAPER

fetuses with Hb Bart's anemia from unaffected fetuses, achieving a sensitivity of 100%, specificity of 98.7% and overall accuracy of 99.1%.

Conclusions Speckle-tracking analysis of the fetal heart has the potential to accurately identify early fetal cardiac changes during the second trimester in individuals with Bart's anemia. These findings not only offer a novel predictive marker for Hb Bart's anemia, but also help address the question of the underlying mechanisms of heart failure associated with fetal anemia. © 2024 The Author(s). Ultrasound in Obstetrics & Gynecology published by John Wiley & Sons Ltd on behalf of International Society of Ultrasound in Obstetrics and Gynecology.

INTRODUCTION

Hemoglobin (Hb) Bart's disease, or homozygous alpha (α)-thalassemia-1, is a prevalent cause of fetal anemia and hydrops fetalis in Southeast Asia, contributing to 30% of hydropic fetuses in Thailand[1,2]. The definitive diagnosis involves invasive prenatal testing, such as chorionic villus sampling, amniocentesis or cordocentesis, which carries a risk of pregnancy loss. In order to minimize the associated risks and potential medical expense of invasive testing[3], some couples opt for serial ultrasound surveillance, avoiding an invasive procedure unless there is evidence of fetal hydrops.

There are several sonographic markers used to identify affected fetuses, including increased fetal cardiothoracic (CT) ratio and peak systolic velocity in the middle cerebral artery (MCA-PSV). Although these markers exhibit high sensitivity, their specificity ranges widely[4–8]. Combining markers enhances sensitivity but results in modest specificity[7,9,10]. Fetal speckle-tracking analysis of the size, shape and contractility of the right and left ventricles has been applied in various fetal conditions but not in Hb Bart's disease[11–17].

Fetuses with Hb Bart's disease respond to anemia by increasing cardiac size and output, likely due to reduced blood viscosity, leading to increased venous return and preload. This cascade may result in cardiac failure and hydrops fetalis[4]. Previous studies revealed that in cases of hydrops fetalis secondary to fetal anemia, the initial cause is hypervolemia rather than ventricular diastolic dysfunction. However, ventricular diastolic compromise tends to occur later as a consequence of persistent hypervolemia and prolonged overworking of the heart[18,19].

Fetal speckle-tracking analysis could serve as a predictive marker and provide insights into the pathophysiology of anemia-induced heart failure. Despite the fatal nature of Hb Bart's disease, studying the fetal cardiac response before hydropic onset offers valuable insight that may be applicable to non-lethal causes of fetal anemia, such as rhesus isoimmunization and parvovirus B19 infection[4,5]. Improved understanding of fetal adaptations to anemia could lead to enhanced care through improved prenatal diagnosis, intrauterine intervention or timely delivery.

Establishing normative values is crucial for identifying fetal Hb Bart's anemia. Previously, we compiled fetal speckle-tracking data for the Thai population at 17–24 gestational weeks[20,21]. This study aimed to assess the diagnostic performance of fetal cardiac measurements derived from speckle-tracking echocardiography for distinguishing between fetuses affected by Hb Bart's disease and unaffected fetuses in pregnancies at risk during mid-gestation.

METHODS

From January 2019 to January 2021, this prospective cohort study was conducted in pregnant women identified as being at risk for fetal Hb Bart's disease who underwent amniocentesis or cordocentesis for prenatal diagnosis in the Division of Maternal-Fetal Medicine (MFM), Department of Obstetrics and Gynecology, Siriraj Hospital, Mahidol University, Bangkok, Thailand. This study was approved by the institutional review board of Siriraj Ethics Committee (COA no. Si 814/2018) and written informed consent to participate was obtained from all patients involved in the study.

Study population

Inclusion criteria were maternal age of at least 18 years and singleton pregnancy at 17–24 gestational weeks based on the last menstrual period and a confirmed ultrasound examination during the first or second trimester. Fetuses were identified as having a risk of Hb Bart's disease by maternal and paternal thalassemia blood-test screening and were scheduled for prenatal diagnosis by either amniocentesis or cordocentesis for fetal α-globin gene or Hb typing. Exclusion criteria included fetal structural or chromosomal abnormality. Each fetus underwent a single ultrasound examination for the purposes of this study. Cases in which an adequate fetal four-chamber view (4CV) was unobtainable and those lacking results from invasive prenatal testing were withdrawn from the study. Hydrops fetalis was defined as the presence of at least two abnormal fluid collections, such as pleural or pericardial effusions or ascites, or fluid accumulation in one cavity and anasarca. All ultrasound findings were acquired before the invasive testing results were available. Confirmatory diagnosis of Hb Bart's disease was based on either fetal DNA amplification by polymerase chain reaction for α-globin gene analysis following amniocentesis or Hb typing using high-performance liquid chromatography and α-globin gene analysis following cordocentesis.

After the prenatal diagnostic results had been obtained, two study groups were identified: an affected group, with a confirmed diagnosis of Hb Bart's disease, and an unaffected (control) group, which included cases with normal α-globin gene, α-thalassemia-1 trait, α-thalassemia-2 trait, Hb H disease or Hb H constant spring or Pakse disease. The affected group was further subdivided into those with and those without hydrops fetalis.

Ultrasound image acquisition and orientation

Before performing amniocentesis/cordocentesis for fetal α-globin gene or Hb typing, two-dimensional (2D) ultrasound images of the 4CV were obtained using a Voluson E10 (GE Healthcare, Zipf, Austria) ultrasound machine, equipped with either a C1-5-D or a RAB6-D transducer. Images were optimized to enhance the borders between the blood pool and endocardium. Three-second cineclips of the 4CV were stored as Digital Imaging and Communications in Medicine (DICOM) files and exported to an offline cloud database. The DICOM image frame rate was equivalent to the acquisition frame rate at the time of the examination, in which the mean number of frames per cardiac cycle was > 40. The apex of the 4CV varied according to the fetal position, with no view analyzed with the apex at 6 o'clock. Irrespective of the orientation of the 4CV, the criteria for speckle-tracking analysis required the endocardial borders of the lateral and septal walls of each ventricle to be identified adequately. The videoclips of the 4CV were recorded by one of two MFM specialists (S.A. and K.R.), while all speckle-tracking measurements were performed by a single examiner (G.R.D.) with expertise in fetal echocardiography and speckle-tracking analysis, who was blinded to the results of the prenatal diagnosis.

Measurements of epicardial shape and size of four-chamber view

Using a DICOM measurement package (Escape Medical Viewer, Thessaloniki, Greece), linear measurements in the 4CV were performed for each fetus. These consisted of the end-diastolic basal–apical length, measured as the largest dimension from epicardium to epicardium, and the end-diastolic transverse width, measured from epicardium to epicardium at the point of the largest width (Figure 1)[20]. From these measurements, the global sphericity index (GSI) was calculated by dividing the end-diastolic basal–apical length by the end-diastolic transverse width[20]. Values below the 50th percentile of the GSI suggested a more globular shape of the heart, whereas values above the 50th percentile suggested flattening of the heart[22]. To measure the size of the 4CV, the end-diastolic area and circumference were measured using two techniques. The first involved tracing the epicardial contour of the 4CV using a point-to-point trace method (Figure 1)[20]. For the second, the area and circumference were calculated from the end-diastolic length and width measurements as follows[20]:

1. Area = (3.14159 × length × width)/4
2. Circumference = 3.14 × ((length/2) + (width/2)) × 1 + (3 × ((length/2) − (width/2))/((length/2) + (width/2)))ˆ2/(10 + (SQRT((4 − 3 × ((length/2) − (width/2)) + (length/2 + width))ˆ2)))).

Right and left ventricular endocardial measurements derived from speckle-tracking analysis

2D images of the 4CV, stored in DICOM format, were imported into an offline cardiac software program (2D
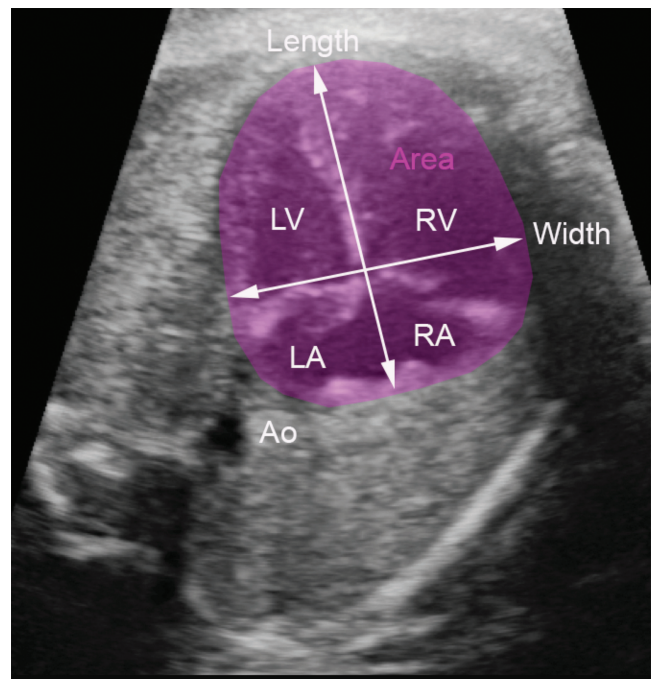

Figure 1 Measurements of the fetal four-chamber view (purple shading): end-diastolic area, circumference, length and width. Right (RA) and left (LA) atria and right (RV) and left (LV) ventricles are indicated. Ao, descending aorta.

Cardiac Performance Analysis or 2D CPA), developed by TomTec Imaging Systems, GMBH (Munich, Germany), using criteria for fetal applications that have been described previously[14]. The following measurements of endocardial ventricular shape, size and contractility were computed from the speckle-tracking analysis from a single cardiac cycle (Figure 2).

Right and left end-diastolic ventricular shape

The 24 segment sphericity indices were computed by dividing the end-diastolic length of the ventricular chamber by the end-diastolic length of each of the 24 transverse segments (Figure 2a).

Right and left end-diastolic ventricular size

The end-diastolic area was calculated according to Anuwutnavin *et al.*[20] (Figure 2b). The end-diastolic length was measured for each of the 24 transverse segments (Figure 2a).

Ratio of end-diastolic areas

The ratio of the end-diastolic areas was computed by dividing the right ventricular end-diastolic area by the left ventricular end-diastolic area (mean (computed from the 85 control fetuses), 0.80; SD, 0.20)[20] (Figure 2b).

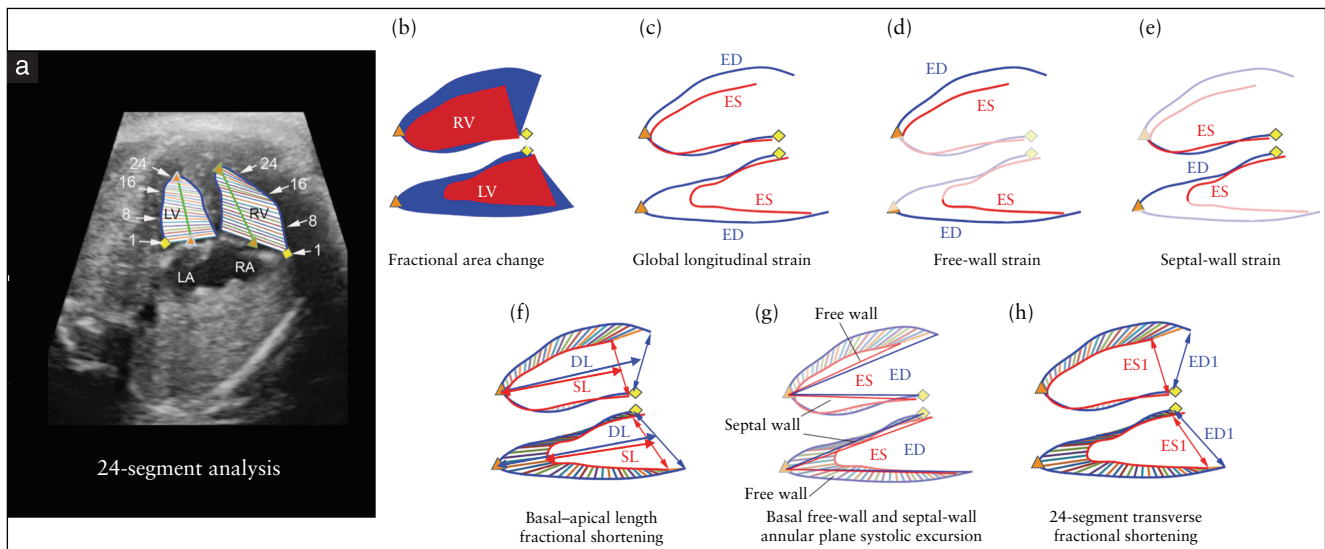### *Right and left ventricular contractility*

Ventricular contractility was defined by non-volume measurements of the ventricles and categorized as follows:

(1) global contractility; (2) longitudinal contractility; and (3) transverse contractility. Global contractility was ascertained by measuring the fractional area change (FAC) (Table 1 and Figure 2b). Longitudinal contractility was divided into three sections: (1) global, free-wall and septal-wall longitudinal strain (Table 1 and Figure 2c–e); (2) basal–apical length fractional shortening (Table 1 and Figure 2f); and (3) free-wall and septal-wall annular plane systolic excursion (Table 1 and Figure 2g). Transverse contractility, defined as transverse fractional shortening,

was computed for each of the 24 transverse segments (Table 1 and Figure 2h).

Left ventricular function

Left ventricular function was defined by end-systolic and end-diastolic volume measurements of the left ventricle, computed, using Simpson's rule[23], from the 24 segment transverse volume measurements (Table 2 and Figure 2a). The volume measurements were used to compute the

Figure 2 Speckle-tracking measurements of the ventricles and graphic illustration of end-systolic and end-diastolic measurements used to compute ventricular contractility[21]. (a) Ultrasound image illustrating the 24 end-diastolic transverse segments for the right (RV) and left (LV) ventricles and their corresponding mid-chamber lengths. (b–h) Schematic diagrams illustrating: (b) fractional area change; (c) global longitudinal strain; (d) free-wall strain; (e) septal-wall strain; (f) basal–apical length fractional shortening; (g) basal free-wall and septal-wall annular plane systolic excursion; and (h) 24-segment transverse fractional shortening. Blue indicates end-diastolic measurements and red indicates end-systolic measurements. Yellow diamonds indicate septal wall markers and orange triangles indicate the apex. DL, diastolic length; ED, end diastole; ED1, end-diastolic width for segment 1; ES, end systole; ES1, end-systolic width for segment 1; LA, left atrium; RA, right atrium; SL, systolic length.

Table 1 Measurements of right and left ventricular contractility[21]

Measurement	Figure	Equation
Global contractility		
Fractional area change	2b	((End-diastolic area − end-systolic area)/end-diastolic area) × 100
Longitudinal contractility		
Strain		
Global longitudinal	2c	((End-systolic endocardial length − end-diastolic endocardial length)/end-diastolic endocardial length) × 100
Free wall	2d	((End-systolic endocardial free-wall length − end-diastolic endocardial free-wall length)/end-diastolic endocardial free-wall length) × 100
Septal wall	2e	((End-systolic endocardial septal-wall length − end-diastolic endocardial septal-wall length)/end-diastolic endocardial septal-wall length) × 100
Basal–apical length fractional shortening	2f	((End-diastolic mid-chamber length − end-systolic mid-chamber length)/end-diastolic mid-chamber length) × 100
Annular plane systolic excursion		
Free wall	2g	(End-diastolic free-wall length measured from apex to annular base − end-systolic free-wall length measured from apex to annular base)
Septal wall	2g	(End-diastolic septal-wall length measured from apex to annular base − end-systolic septal-wall length measured from apex to annular base)
Transverse contractility		
24-segment transverse fractional shortening	2h	((End-diastolic width − end-systolic width)/end-diastolic width) × 100

stroke volume, cardiac output and ejection fraction (Table 2).

Statistical analysis

Demographic data are presented as n (%) and mean $\pm$ SD, as appropriate. Continuous variables were compared between groups using the unpaired t-test and among groups using one-way ANOVA, followed by *post-hoc* tests with Bonferroni correction. Categorical variables were compared by Pearson's χ^2 or Fisher's exact test. Univariable analysis was performed to assess cardiac parameters associated with Hb Bart's anemia. Results were presented as mean Z-score $\pm$ SD using the NCSS version 22 statistical software package (NCSS, Kaysville, Utah, USA). $P < 0.05$ was considered to indicate statistical significance.

Logistic regression analysis

Equations derived from fractional polynomial regression analysis in our previous two studies[20,21] were employed to determine normal mean and SD values of the 18 cardiac measurements using the head circumference (HC), biparietal diameter (BPD), abdominal circumference (AC), femur length (FL), estimated fetal weight (EFW) and gestational age as the independent variable. These equations enabled the computation of Z-scores for each of the 18 cardiac measurements, which were then converted to percentiles. Using the Z-score values, multivariable logistic regression analysis was performed to identify the variables and their coefficients that were predictive of Hb Bart's disease (NCSS version 22 statistical software). Each of the identified cardiac variables was tested for its ability to differentiate between the non-hydropic fetuses with Hb Bart's disease and the controls. The diagnostic values were reported as sensitivity, specificity, positive predictive value, negative predictive value, false-positive rate, false-negative rate and accuracy. The final multivariable logistic model was used to calculate the probability for Bart's anemia from the logit value of each patient and we then converted the value to a probability value. A probability of $>50\%$ was considered diagnostic of Hb Bart's anemia.

Comparison with other ultrasound measurements

Previous studies have reported CT diameter ratio > 0.5[3,6,10,24,25], MCA-PSV > 1.5 multiples of the median (MoM)[7,8,10,26] and a placental thickness > 3 cm[6,10,27] to be indicators of fetal Bart's anemia. Their diagnostic performance in the prediction of non-hydropic fetuses with Hb Bart's anemia, compared with that of the fetal cardiac measurements, was assessed by calculating their sensitivity, specificity, positive predictive value, negative predictive value, false-positive rate, false-negative rate and accuracy, and by receiver-operating-characteristics (ROC)-curve analysis.

RESULTS

During the study period, 119 pregnancies at risk for fetal Hb Bart's disease were enrolled prospectively into the study. Of these 119 fetuses, 115 (96.6%) had 4CV images that were suitable for speckle-tracking analysis and were included in the analysis. Maternal ethnicities comprised 110 Thai (95.7%), three Laos (2.6%), one Burmese (0.9%) and one Cambodian (0.9%). The mean $\pm$ SD maternal age was 28.77 ± 5.83 years and gestational age was 18.98 ± 1.43 weeks. Just over half (52.2%) of the study participants were nulliparous.

A fetal α-globin gene study following amniocentesis was carried out in 90 (78.3%) cases and Hb typing and fetal α-globin gene study following cordocentesis in 25 (21.7%), to determine which fetuses had Hb Bart's disease. There were 38 (33.0%) fetuses with Hb Bart's disease and 77 (67.0%) fetuses without. These unaffected pregnancies formed the control group and included fetuses with normal α-globin gene, α-thalassemia-1 trait, α-thalassemia-2 trait and α-thalassemia intermedia, such as Hb H disease and Hb H constant spring or Pakse disease (19.5%, 62.3%, 3.9%, and 14.3%, respectively). Nine (23.7%) cases with Hb Bart's disease demonstrated clear hydropic signs, such as pericardial effusion, pleural effusion, ascites and anasarca.

There were no significant differences between the group of fetuses affected by Hb Bart's disease and the control group in maternal age, gestational age, parity, underlying maternal disease, type of parental α-globin genes and presence of abnormal β-globin gene in either of the parents or in the fetuses (Table S1).

Four-chamber view size and shape

Table 3 presents the mean Z-scores and corresponding Z-score percentiles for the 4CV measurements. When

Table 2 Left ventricular function measurements

Measurement	Figure	Equation
Left ventricular end-diastolic and end-systolic volumes	2a	Computed using Simpson's rule from the 24 segment end-diastolic and end-systolic transverse width measurements and lengths*
Left ventricular stroke volume	2a	(End-diastolic volume − end-systolic volume)
Left ventricular cardiac output	2a	(Heart rate × stroke volume)
Left ventricular ejection fraction	2a	((End-diastolic volume − end-systolic volume)/end-diastolic volume) × 100

*End-diastolic and end-systolic volumes were computed using speckle-tracking software by the Simpson method of disk analysis[23], in which the area of each of the 24 segments was multiplied by each of the 24 segment lengths (between transverse segments; Figure 2a, left ventricle).

compared with controls, both the non-hydropic and hydropic fetuses showed significantly higher mean Z-scores for the 4CV area, circumference, width and length, but not the GSI. When compared with the non-hydropic fetuses, the hydropic fetuses had a significantly increased mean Z-score for 4CV area, circumference, width and length.

Ventricular size, shape and contractility: controls vs *non-hydropic fetuses with Hb Bart's disease*

Table 4 compares the control group to the non-hydropic fetuses with Hb Bart's disease.

For the right ventricle, the mean Z-scores of the end-diastolic area, base width and mid-chamber width in non-hydropic fetuses were significantly greater than those of controls, while the mean Z-scores of the base and mid-chamber sphericity indices were borderline significantly lower, indicating a potentially globular-shaped right ventricular chamber. However, no statistically significant differences were observed in terms of global, longitudinal and transverse contractility between the controls and the non-hydropic fetuses with Hb Bart's disease.

For the left ventricle, the mean Z-score for the global contractility measurement of FAC in non-hydropic fetuses was significantly lower than that of the controls. Of the longitudinal contractility measurements, the mean Z-score values for both global longitudinal and free-wall strain were significantly higher, while those for basal–apical length fractional shortening were significantly lower in non-hydropic fetuses compared with controls. Additionally, the mean Z-score of the ejection fraction was significantly lower in non-hydropic fetuses compared with controls. However, there was no significant indication of a globular-shaped chamber for the left ventricle.

Ventricular size, shape and contractility: controls vs *hydropic fetuses with Hb Bart's disease*

Table 5 compares the control group to the hydropic fetuses with Hb Bart's disease.

For the right ventricle, only the mean Z-score of the end-diastolic area in hydropic fetuses was significantly greater than that of controls.

For the left ventricle, the mean Z-scores for the end-diastolic base width and mid-chamber width in hydropic fetuses were significantly greater than those of the controls. Of the contractility measurements, only the mean Z-score of the free-wall strain was significantly different between the groups, being greater (representing decreased contractility) in hydropic fetuses with Hb Bart's disease compared to controls.

Ventricular size, shape and contractility: non-hydropic vs *hydropic fetuses with Hb Bart's disease*

Table 6 compares the non-hydropic *vs* the hydropic fetuses with Hb Bart's disease.

For the right ventricle, compared to the hydropic fetuses, the non-hydropic fetuses had a significantly greater mean Z-score for the base and mid-chamber width.

For the left ventricle, there was no significant difference between the non-hydropic and hydropic fetuses for any measurement.

Predicting the probability of non-hydropic fetuses having Hb Bart's disease

Table 7 presents the results of the logistic regression analysis for identifying non-hydropic fetuses with Hb Bart's disease ($n = 29$). Of the six independent variables used to compute the cardiac Z-scores, HC had the highest sensitivity (100.0% (95% CI, 86.0–100.0%)), with a specificity of 98.7% (95% CI, 91.0–99.0%). The positive predictive value for HC was 96.7% (95% CI, 89.0–99.0%), the negative predictive value was 100.0% (95% CI, 95.0–100.0%), the false-positive rate was 1.3% (95% CI, 0.2–7.0%) and the false-negative rate was 0% (95% CI, 0.0–10.0%), with an accuracy of 99.1% (95% CI, 95.0–100.0%). Table 8 lists the 14 cardiac measurements and their regression coefficients derived from the logistic regression analysis which were used to compute the probability of Hb Bart's disease for each of the 29 non-hydropic fetuses with Hb Bart's disease and the 77 unaffected controls. Appendix S1 gives the individual probability for each of these fetuses and demonstrates that the logistic regression equation correctly identified 100% of fetuses which had Hb Bart's disease, with only one false-positive case from the control group.

Table 3 Comparison of Z-scores of four-chamber view measurements during end diastole among control fetuses and non-hydropic and hydropic fetuses with hemoglobin (Hb) Bart's disease

Measurement	Controls (n = 77)	Non-hydropic Hb Bart's (n = 29)	Hydropic Hb Bart's (n = 9)	P* Control vs non-hydropic	Control vs hydropic	Non-hydropic vs hydropic
Two-diameter area Z-score	0.24 ± 1.20; p59	1.89 ± 1.46; p97	3.82 ± 1.30; p99.9	< 0.001	< 0.001	0.001
Two-diameter circumference Z-score	0.08 ± 1.00; p53	1.67 ± 0.90; p95	3.02 ± 0.90; p99.9	< 0.001	< 0.001	0.003
Width Z-score	0.61 ± 1.16; p52	2.62 ± 1.35; p99	3.92 ± 1.00; p99.9	< 0.001	< 0.001	0.017
Length Z-score	−0.15 ± 1.00; p44	0.94 ± 1.00; p83	2.13 ± 0.88; p98	< 0.001	< 0.001	0.012
GSI Z-score	−0.92 ± 1.40; p18	−1.63 ± 2.00; p5	−1.49 ± 1.00; p7	0.139	0.948	1.00

Data are given as mean ± SD; percentile (p). *ANOVA with Bonferroni correction. GSI, global sphericity index.

Table 4 Comparison of Z-scores of measurements of ventricular size, shape and contractility between control fetuses and non-hydropic fetuses with hemoglobin (Hb) Bart's disease

Measurement	Right ventricle			Left ventricle		
	Controls (n = 77)	*Non-hydropic Hb Bart's* (n = 29)	P*	*Controls* (n = 77)	*Non-hydropic Hb Bart's* (n = 29)	P*
Size and shape						
Area Z-score	−0.50 ± 1.14; p31	0.61 ± 1.66; p73	0.001	−0.02 ± 0.10; p49	−0.01 ± 0.02; p50	0.986
Length Z-score	−0.39 ± 1.12; p35	−0.86 ± 1.21; p19	0.46	−0.13 ± 1.00; p45	−0.22 ± 0.99; p41	1.00
Base width (Segment 1) Z-score	−0.21 ± 1.34; p42	1.07 ± 1.42; p86	<0.001	0.13 ± 1.33; p55	0.81 ± 1.81; p79	0.163
Mid-chamber width (Segment 12) Z-score	0.47 ± 1.47; p68	2.33 ± 1.66; p99	<0.001	−0.14 ± 1.03; p44	0.40 ± 1.11; p66	0.121
Base sphericity index (Segment 1) Z-score	−0.35 ± 0.99; p36	−0.89 ± 0.97; p19	0.045	−0.49 ± 1.00; p31	−0.81 ± 1.27; p21	0.603
Mid-chamber sphericity index (Segment 12) Z-score	−0.69 ± 1.00; p25	−1.22 ± 0.96; p11	0.05	−0.37 ± 1.10; p36	−0.87 ± 1.00; p19	0.162
Global contractility						
Fractional area change Z-score	−0.40 ± 1.44; p34	−1.12 ± 1.32; p13	0.074	−0.66 ± 1.51; p25	−1.86 ± 2.20; p3	0.008
Longitudinal contractility						
Global longitudinal strain Z-score	0.17 ± 1.55; p57	0.64 ± 1.46; p74	0.534	0.02 ± 1.40; p51	1.01 ± 1.67; p84	0.009
Free-wall strain Z-score	0.02 ± 1.38; p51	0.55 ± 1.27; p71	0.228	0.01 ± 1.48; p50	0.85 ± 1.35; p80	0.027
Septal-wall strain Z-score	−0.05 ± 1.20; p48	0.35 ± 1.48; p64	0.469	0.01 ± 1.26; p50	0.57 ± 1.42; p72	0.155
Basal–apical length fractional shortening Z-score	0.04 ± 1.65; p52	−0.66 ± 1.54; p25	0.152	0.07 ± 1.29; p53	−0.79 ± 1.57; p21	0.016
Free-wall annular plane systolic excursion Z-score	−0.71 ± 1.05; p24	−0.69 ± 1.55; p25	1.00	−0.95 ± 1.01; p17	−1.25 ± 0.90; p11	0.454
Septal-wall annular plane systolic excursion Z-score	0.47 ± 1.10; p68	0.48 ± 1.62; p68	1.00	−0.58 ± 1.09; p28	−0.72 ± 1.23; p24	1.00
Transverse contractility						
Base fractional shortening (Segment 1) Z-score	−0.05 ± 1.16; p48	−0.17 ± 1.26; p43	1.00	−0.12 ± 1.26; p45	−0.56 ± 1.22; p29	0.37
Mid-chamber fractional shortening (Segment 12) Z-score	0.19 ± 1.38; p58	−0.15 ± 1.10; p44	0.743	−0.62 ± 1.12; p27	−1.25 ± 1.44; p11	0.061
Left ventricular function						
Stroke volume Z-score	—	—	—	0.20 ± 3.90; p58	0.31 ± 5.32; p62	1.00
Cardiac output Z-score	—	—	—	−0.11 ± 1.70; p46	−0.65 ± 1.70; p15	0.12
Ejection fraction Z-score	—	—	—	−0.83 ± 1.83; p20	−2.44 ± 3.40; p1	0.007

Data are given as mean ± SD; percentile (p). *ANOVA with Bonferroni correction.

Table 5 Comparison of Z-scores of measurements of ventricular size, shape and contractility between control fetuses and hydropic fetuses with hemoglobin (Hb) Bart's disease

	Right ventricle			*Left ventricle*		
Measurement	*Controls* (n = 77)	*Hydropic Hb Bart's* (n = 9)	P*	*Controls* (n = 77)	*Hydropic Hb Bart's* (n = 9)	P*
Size and shape						
Area Z-score	−0.50 ± 1.14; p31	0.69 ± 1.50; p75	0.035	−0.02 ± 0.10; p49	−0.02 ± 0.12; p49	0.647
Length Z-score	−0.39 ± 1.12; p35	−0.80 ± 2.00; p21	1.00	−0.13 ± 1.00; p45	0.16 ± 0.96; p56	1.00
Base width (Segment 1) Z-score	−0.21 ± 1.34; p42	−0.57 ± 2.57; p28	1.00	0.13 ± 1.33; p55	1.75 ± 2.60; p96	0.013
Mid-chamber width (Segment 12) Z-score	0.47 ± 1.47; p68	0.11 ± 3.10; p54	1.00	−0.14 ± 1.03; p44	0.97 ± 2.30; p83	0.029
Base sphericity index (Segment 1) Z-score	−0.35 ± 0.99; p36	−0.07 ± 1.25; p47	1.00	−0.49 ± 1.00; p31	−0.97 ± 1.60; p17	0.695
Mid-chamber sphericity index (Segment 12) Z-score	−0.69 ± 1.00; p25	−0.64 ± 0.92; p26	1.00	−0.37 ± 1.10; p36	−0.68 ± 1.90; p25	1.00
Global contractility						
Fractional area change Z-score	−0.40 ± 1.44; p34	−0.66 ± 1.97; p25	1.00	−0.66 ± 1.51; p25	−1.85 ± 2.40; p3	0.182
Longitudinal contractility						
Global longitudinal strain Z-score	0.17 ± 1.55; p57	1.21 ± 1.97; p89	0.185	0.02 ± 1.40; p51	1.12 ± 1.70; p87	0.117
Free-wall strain Z-score	0.02 ± 1.38; p51	0.43 ± 1.26; p67	1.00	0.01 ± 1.48; p50	1.45 ± 1.64; p93	0.018
Septal-wall strain Z-score	−0.05 ± 1.20; p48	0.07 ± 1.30; p53	1.00	0.01 ± 1.26; p50	0.32 ± 1.49; p63	1.00
Basal–apical length fractional shortening Z-score	0.04 ± 1.65; p52	−0.73 ± 1.78; p23	0.607	0.07 ± 1.29; p53	−0.93 ± 1.59; p18	0.128
Free-wall annular plane systolic excursion Z-score	−0.71 ± 1.05; p24	−1.53 ± 1.15; p6	0.163	−0.95 ± 1.01; p17	−1.50 ± 0.80; p7	0.326
Septal-wall annular plane systolic excursion Z-score	0.47 ± 1.10; p68	−0.39 ± 1.20; p35	0.163	−0.58 ± 1.09; p28	−0.16 ± 1.80; p44	0.953
Transverse contractility						
Base fractional shortening (Segment 1) Z-score	−0.05 ± 1.16; p48	−0.69 ± 1.53; p25	0.469	−0.12 ± 1.26; p45	−0.30 ± 1.79; p38	1.00
Mid-chamber fractional shortening (Segment 12) Z-score	0.19 ± 1.38; p58	−0.20 ± 1.70; p42	1.00	−0.62 ± 1.12; p27	−1.05 ± 1.33; p15	0.955
Left ventricular function						
Stroke volume Z-score	—	—	—	0.20 ± 3.90; p58	1.28 ± 3.98; p90	1.00
Cardiac output Z-score	—	—	—	−0.11 ± 1.70; p46	0.45 ± 2.39; p67	1.00
Ejection fraction Z-score	—	—	—	−0.83 ± 1.83; p20	−1.32 ± 2.10; p9	0.291

Data are given as mean ± SD; percentile (p). *ANOVA with Bonferroni correction.

Table 6 Comparison of Z-scores of measurements of ventricular size, shape and contractility between non-hydropic and hydropic fetuses with hemoglobin (Hb) Bart's disease

Measurement	Right ventricle			Left ventricle		
	Non-hydropic Hb Bart's (n = 29)	*Hydropic Hb Bart's (n = 9)*	*P**	*Non-hydropic Hb Bart's (n = 29)*	*Hydropic Hb Bart's (n = 9)*	*P**
Size and shape						
Area Z-score	0.61 ± 1.66; p73	0.69 ± 1.50; p75	1.00	−0.01 ± 0.02; p50	−0.02 ± 0.12; p49	1.00
Length Z-score	−0.86 ± 1.21; p19	−0.80 ± 2.00; p21	1.00	−0.22 ± 0.99; p41	0.16 ± 0.96; p56	0.959
Base width (Segment 1) Z-score	1.07 ± 1.42; p86	−0.57 ± 2.57; p28	0.013	0.81 ± 1.81; p79	1.75 ± 2.60; p96	0.36
Mid-chamber width (Segment 12) Z-score	2.33 ± 1.66; p99	0.11 ± 3.10; p54	0.002	0.40 ± 1.11; p66	0.97 ± 2.30; p83	0.646
Base sphericity index (Segment 1) Z-score	−0.89 ± 0.97; p19	−0.07 ± 1.25; p47	0.131	−0.81 ± 1.27; p21	−0.97 ± 1.60; p17	1.00
Mid-chamber sphericity index (Segment 12) Z-score	−1.22 ± 0.96; p11	−0.64 ± 0.92; p26	0.428	−0.87 ± 1.00; p19	−0.68 ± 1.90; p25	1.00
Global contractility						
Fractional area change Z-score	−1.12 ± 1.32; p13	−0.66 ± 1.97; p25	1.00	−1.86 ± 2.20; p3	−1.85 ± 2.40; p3	1.00
Longitudinal contractility						
Global longitudinal strain Z-score	0.64 ± 1.46; p74	1.21 ± 1.97; p89	1.00	1.01 ± 1.67; p84	1.12 ± 1.70; p87	1.00
Free-wall strain Z-score	0.55 ± 1.27; p71	0.43 ± 1.26; p67	1.00	0.85 ± 1.35; p80	1.45 ± 1.64; p93	0.867
Septal-wall strain Z-score	0.35 ± 1.48; p64	0.07 ± 1.30; p53	1.00	0.57 ± 1.42; p72	0.32 ± 1.49; p63	1.00
Basal–apical length fractional shortening Z-score	−0.66 ± 1.54; p25	−0.73 ± 1.78; p23	1.00	−0.79 ± 1.57; p21	−0.93 ± 1.59; p18	1.00
Free-wall annular plane systolic excursion Z-score	−0.69 ± 1.55; p25	−1.53 ± 1.15; p6	0.211	−1.25 ± 0.90; p11	−1.50 ± 0.80; p7	1.00
Septal-wall annular plane systolic excursion Z-score	0.48 ± 1.62; p68	−0.39 ± 1.20; p35	0.211	−0.72 ± 1.23; p24	−0.16 ± 1.80; p44	0.675
Transverse contractility						
Base fractional shortening (Segment 1) Z-score	−0.17 ± 1.26; p43	−0.69 ± 1.53; p25	0.857	−0.56 ± 1.22; p29	−0.30 ± 1.79; p38	1.00
Mid-chamber fractional shortening (Segment 12) Z-score	−0.15 ± 1.10; p44	−0.20 ± 1.70; p42	1.00	−1.25 ± 1.44; p11	−1.05 ± 1.33; p15	1.00
Left ventricular function						
Stroke volume Z-score	—	—	—	0.31 ± 5.32; p62	1.28 ± 3.98; p90	1.00
Cardiac output Z-score	—	—	—	−0.65 ± 1.70; p15	0.45 ± 2.39; p67	0.156
Ejection fraction Z-score	—	—	—	−2.44 ± 3.40; p1	−1.32 ± 2.10; p9	1.00

Data are given as mean ± SD; percentile (p). *ANOVA with Bonferroni correction.

Table 7 Diagnostic performance of 14 fetal echocardiographic measurements* derived from speckle-tracking analysis for identifying non-hydropic fetuses with hemoglobin Bart's disease ($n = 29$) according to six independent variables

Independent variable	Sensitivity	Specificity	PPV	NPV	FPR	FNR	Accuracy
HC (in cm)	100.0 (86.0–100.0)	98.7 (91.0–99.0)	96.7 (89.0–99.0)	100.0 (95.0–100.0)	1.3 (0.2–7.0)	0.0 (0.0–10.0)	99.1 (95.0–100.0)
BPD (in cm)	82.8 (64.0–94.0)	93.5 (85.0–98.0)	82.8 (67.0–92.0)	93.5 (87.0–97.0)	6.5 (3.0–10.0)	17.2 (8.0–30.0)	90.6 (83.0–95.0)
AC (in cm)	75.9 (56.0–90.0)	97.4 (91.0–100.0)	91.7 (73.0–98.0)	91.5 (85.0–95.0)	2.6 (0.7–9.0)	24.1 (10.0–40.0)	91.5 (85.0–96.0)
FL (in cm)	96.6 (82.0–100.0)	97.4 (91.0–100.0)	93.3 (78.0–98.0)	98.7 (92.0–100.0)	2.6 (0.7–9.0)	3.5 (0.6–20.0)	97.2 (92.0–99.0)
EFW (in g)	86.2 (68.0–96.0)	97.4 (91.0–100.0)	92.6 (76.0–98.0)	94.9 (88.0–98.0)	2.6 (0.7–9.0)	13.8 (5.0–30.0)	94.3 (88.0–98.0)
GA (in weeks)	82.8 (64.0–94.0)	97.4 (91.0–100.0)	92.3 (75.0–99.0)	93.8 (87.0–97.0)	2.6 (0.7–9.0)	17.2 (8.0–30.0)	93.4 (87.0–97.0)

Data are given as % (95% CI). *For echocardiographic measurements see 14 independent variables given in Table 8. AC, abdominal circumference; BPD, biparietal diameter; EFW, estimated fetal weight; FL, femur length; FNR, false-negative rate; FPR, false-positive rate; GA, gestational age; HC, head circumference; NPV, negative predictive value; PPV, positive predictive value.

Table 8 Logistic regression coefficients for predicting hemoglobin Bart's disease in non-hydropic fetuses, estimated as a function of head circumference

Independent variable	Regression coefficient	Standard error	Lower 95% CL	Upper 95% CL
Intercept	24.23119	4.99232	14.44643	34.01595
Four-chamber view				
Width Z-score	−17.39194	6.37644	−29.88954	−4.89433
Two-diameter area Z-score	15.08256	3.86919	7.49908	22.66603
Two-diameter circumference Z-score	−8.99803	6.44864	−21.63713	3.64108
Global sphericity index Z-score	−5.16705	2.59736	−10.25779	−0.07631
Ventricular size				
LV area Z-score	76.03863	17.04885	42.62351	109.45376
RV area Z-score	−10.42078	2.49278	−15.30654	−5.53501
RV length Z-score	13.83349	3.45013	7.07136	20.59562
RV diameter Segment 1 Z-score	−3.42594	0.99286	−5.37191	−1.47998
Ventricular shape (sphericity index)				
RV base Segment 12 Z-score	−11.03336	2.80096	−16.52314	−5.54357
Ventricular contractility				
RV basal–apical length fractional shortening Z-score	6.9916	2.8576	1.39081	12.5924
RV transverse fractional shortening Segment 12 Z-score	−8.7263	1.99607	−12.63852	−4.81409
RV fractional area change Z-score	12.62124	2.96751	6.80502	18.43745
LV fractional area change Z-score	1.33063	0.38109	0.5837	2.07756
RV global longitudinal strain Z-score	14.77786	4.30828	6.33379	23.22192

CL, confidence limit of regression coefficient; LV, left ventricle; RV, right ventricle.

Comparison of fetal echocardiographic measurements with other previously reported ultrasound findings in non-hydropic fetuses with Bart's anemia

Table 9 compares the sensitivity, specificity, positive predictive value, negative predictive value, false-positive rate and false-negative rate for the cardiac measurements listed in Table 8, CT diameter ratio > 0.5, MCA-PSV > 1.5 MoM and placental thickness > 3 cm. The fetal cardiac measurements using HC as the independent variable had the highest true-positive rate (100%) and lowest false-positive rate (1.3%) compared with CT diameter ratio > 0.5 (96.6% and 10.4%, respectively), MCA-PSV > 1.5 MoM (96.6% and 11.7%, respectively) and placental thickness > 3 cm (65.5% and 20.8%, respectively). ROC-curve analysis (Figure 3) yielded the following areas under the curves for the diagnostic performance of a probability value for combined cardiac parameters from speckle tracking as a function of HC of > 50%, CT diameter ratio > 0.5, MCA-PSV > 1.5 MoM and placental thickness > 3 cm in the prediction of non-hydropic fetuses with Bart's anemia: 1.000 (95% CI, 1.000–1.000), 0.982 (95% CI, 0.961–1.000), 0.968 (95% CI, 0.938–0.998) and 0.837 (95% CI, 0.750–0.924), respectively.

Table 9 Diagnostic performance of cardiothoracic (CT) diameter ratio, middle cerebral artery peak systolic velocity (MCA-PSV), placental thickness and fetal echocardiographic measurements derived from speckle-tracking analysis in predicting non-hydropic fetuses with hemoglobin Bart's disease ($n = 29$)

Independent variable	Sensitivity	Specificity	PPV	NPV	FPR	FNR	Accuracy
Combined cardiac parameters from speckle tracking as a function of HC*	100.0 (88.1–100.0)	98.7 (93.0–100.0)	96.7 (80.5–99.5)	100.0 (93.5–100.0)	1.3 (0.2–7.0)	0.0 (0.0–12.0)	99.1 (94.9–100.0)
CT diameter ratio > 0.5	96.6 (82.2–99.9)	89.6 (80.6–95.4)	77.8 (64.4–87.1)	98.6 (90.9–99.8)	10.4 (5.4–19.0)	3.4 (0.6–17.0)	91.5 (84.5–96.0)
MCA-PSV > 1.5 MoM	96.6 (82.2–99.9)	88.3 (79.0–94.5)	75.7 (62.7–85.2)	98.6 (90.8–99.8)	11.7 (6.3–21.0)	3.4 (0.6–17.0)	90.6 (83.3–95.4)
Placental thickness > 3 cm	65.5 (45.7–82.1)	79.2 (68.5–87.6)	54.3 (41.6–66.4)	85.9 (78.5–91.1)	20.8 (13.0–31.0)	34.5 (20.0–53.0)	75.5 (66.2–83.3)

Data are given as % (95% CI). *For cardiac parameters see 14 independent variables given in Table 8. FNR, false-negative rate; FPR, false-positive rate; HC, head circumference; MoM, multiples of the median; NPV, negative predictive value; PPV, positive predictive value.
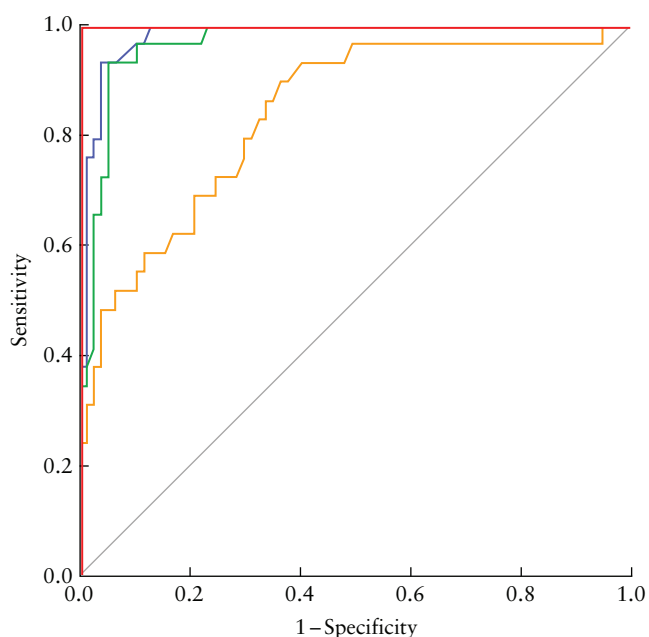
Figure 3 Receiver-operating-characteristics curves for diagnostic performance of cardiothoracic diameter ratio > 0.5 (——), middle cerebral artery peak systolic velocity > 1.5 multiples of the median (——), placental thickness > 3 cm (——) and a probability value for combined fetal echocardiographic measurements derived from speckle-tracking analysis as a function of head circumference of > 50% (——), in predicting non-hydropic fetuses with hemoglobin Bart's disease. Reference line is also shown (——).

DISCUSSION

Thammavong *et al.*[19] reviewed extensively physiological changes in fetal Hb Bart's disease and its sonographic features across gestational stages. Fetal responses progress through three phases: (1) prehydropic (late first trimester to mid-pregnancy), with increased cardiac output and prehydropic signs (cardiomegaly, increased MCA-PSV, placentomegaly); (2) high-output hydropic (mid to late pregnancy), marked by intracellular fluid leakage, causing hydrops fetalis but normal cardiac performance; and (3) low-output hydropic (late pregnancy), when prolonged anemic hypoxia leads to cardiac deterioration. Understanding these phases aids in timely detection of Hb Bart's disease-associated cardiac dysfunction.

Comparison of 2D sonographic findings with speckle tracking in fetal Hb Bart's disease

Non-hydrops fetalis

Corresponding to the prehydropic phase of Thammavong *et al.*[19], the non-hydropic fetuses with Hb Bart's disease in our study exhibited a significant increase in 4CV area, circumference, width and length compared to the control group (Table 3). These findings are consistent with those of prior studies showing fetal cardiomegaly to be a common early morphological change in this stage[19,28]. An elevated CT diameter ratio has been widely used as a 2D ultrasound predictor of fetal Hb Bart's disease[6,7].

Our study discovered that the 4CV GSI did not significantly differ between affected and control fetuses (Table 3). However, a potentially globular shape was observed in the right ventricular chamber in non-hydropic fetuses with Bart's anemia (Table 4). These findings contrast with a previous report showing cardiac remodeling with a significant reduction in 4CV GSI in affected fetuses[4]. Differences may arise from the comparison techniques used, as our study employed mean Z-scores and corresponding percentiles, while the previous study compared mean GSI values directly between groups.

We revealed a significant decrease in global contractility (FAC) for the left ventricle in non-hydropic fetuses with Hb Bart's disease compared with the controls (Table 4). Longitudinal contractility, as measured by strains and basal–apical length fractional shortening, was also markedly lower in these cases than in the controls. The left ventricular ejection fraction also showed a significant reduction in non-hydropic cases. These findings suggest early evidence of abnormal global and longitudinal systolic function in affected fetuses, aligning with previous

2D ultrasonographic studies reporting increased isovolumetric contraction time (ICT) and Tei index in affected fetuses[5,29–33]. Prolonged ICT was a sensitive marker of ventricular systolic dysfunction in response to fetal anemia before the development of ventricular diastolic dysfunction in the late disease stage[5,18,28]. While relying solely on ICT had moderate sensitivity and specificity (71–79%) in detecting Hb Bart's disease during mid-gestation[5], incorporating various cardiac measurements could enhance significantly disease prediction accuracy.

Hydrops fetalis

Corresponding to the high-output hydropic phase of Thammavong *et al.*[19], cases with Hb Bart's hydrops fetalis in our study showed a significantly larger cardiac size compared to both controls and the non-hydropic fetuses with Bart's anemia. Such an increase has been shown to be associated with elevated cardiac output and hypervolemia due to prolonged anemia[28]. The hydropic fetuses in our study displayed Z-score values equal to or exceeding the 98th percentile for 4CV end-diastolic area, circumference, width and length (Table 3).

Cases of Hb Bart's hydrops fetalis exhibited trends towards increased stroke volume and cardiac output compared to control and non-hydropic fetuses, although these differences did not reach statistical significance, likely due to the small sample size (nine cases) in our study. Despite prolonged volume overload, left ventricular function in the hydropic fetuses did not differ significantly from that of the non-hydropic and control groups (Tables 5 and 6). Consistent with prior research[19,28,34,35], fetuses in the high-output hydropic phase maintained normal cardiac function, ensuring sufficient tissue perfusion despite hypervolemia and cardiomegaly. However, once the compensatory mechanism is exhausted, cardiac performance deteriorates in the low-output hydropic phase during late gestation.

Compared with hydropic cases, non-hydropic fetuses with Hb Bart's disease showed a notably greater right ventricular width, especially in the base and mid-chamber regions (Table 6). This probably resulted in a more spherical cardiac shape at the base of the heart. This phenomenon is likely from prolonged volume load, causing myocardial wall stretching stress and eccentric remodeling, leading to the loss of a globular-shaped heart in hydropic fetuses[34]. Additionally, left ventricular free-wall strain, reflecting longitudinal contractility, was significantly higher in the hydropic fetuses than in controls (Table 5), suggesting decreased contractility.

Comparison of diagnostic efficacy of 2D sonographic markers and speckle tracking in detecting fetal Hb Bart's disease

Regarding the diagnostic performance of fetal speckle-tracking echocardiography in predicting Hb Bart's disease, logistic regression analysis identified 14 cardiac variables estimated as a function of HC (Table 8).

This approach detected all affected fetuses, with a low (1.3%) false-positive rate. Compared to studies using CT diameter ratio > 0.5 or MCA-PSV > 1.5 MoM for prediction of Hb Bart's disease[7,9], our study achieved a similar sensitivity (100%) but surpassed them with a lower false-positive rate (1.3% *vs* 10.9–31%). This improvement is likely due to our incorporation of various cardiac parameters. However, in routine practice, CT diameter ratio and MCA-PSV measurements are primary screening tools, while fetal speckle-tracking echocardiography, highlighted herein, acts as a high-specificity secondary predictor, improving diagnostic accuracy. We advise prenatal genetic testing if the probability of Hb Bart's disease exceeds 50%, calculated using our Excel calculator (Appendix S2).

Herein, we present a new screening tool for early detection of fetal Hb Bart's disease, utilizing automated software and a diagnostic Excel calculator. While offering precise identification of at-risk fetuses, limitations of this tool include the requirement for specialized equipment with software and potential difficulties in blinding of the operator to fetal cardiomegaly and pericardial effusion. An evaluation of interobserver reproducibility is lacking, as a single examiner evaluated all cardiac parameters; yet, prior research has documented both intra- and interobserver variability for cardiac measurement by fetal speckle-tracking analysis[36,37]. The study's limited focus on gestational ages between 17 and 24 weeks and the small number of hydropic cases may limit the generalizability and specificity of the results. Moreover, these findings from studying fetal Hb Bart's disease may not be generalizable to anemia from other causes, given the high oxygen affinity of Hb Bart's, causing severe hypoxia without a substantial decrease in Hb levels. Further research should be considered, to validate the speckle-tracking model and to compare its predictive accuracy with that of other 2D ultrasonographic features, such as CT diameter ratio and MCA-PSV measurements.

Conclusions

This is the first study to utilize fetal speckle-tracking analysis to evaluate cardiac changes in response to Hb Bart's disease, comparing findings between unaffected and non-hydropic and hydropic affected fetuses. Use of fetal cardiac measurements as a function of HC demonstrated superior prenatal diagnostic performance over previously described ultrasound markers, identifying accurately early fetal cardiac changes in individuals at risk of developing Bart's anemia.

REFERENCES

1. Taweevisit M, Thorner PS. Hydrops fetalis in the stillborn: a series from the central region of Thailand. *Pediatr Dev Pathol*. 2010;13(5):369-374.
2. Suwanrath-Kengpol C, Kor-anantakul O, Suntharasaj T, Leetanaporn R. Etiology and outcome of non-immune hydrops fetalis in southern Thailand. *Gynecol Obstet Invest*. 2005;59(3):134-137.
3. Lam YH, Ghosh A, Tang MH, Lee CP, Sin SY. Early ultrasound prediction of pregnancies affected by homozygous alpha-thalassaemia-1. *Prenat Diagn*. 1997;17(4):327-332.
4. Tongsong T, Tongprasert F, Srisupundit K, Luewan S, Traisrisilp K, Jatavan P. Fetal cardiac remodeling in response to anemia: using hemoglobin Bart's disease as a study model. *Ultraschall Med*. 2020;41(2):186-191.
5. Tongprasert F, Srisupundit K, Luewan S, Traisrisilp K, Jatavan P, Tongsong T. Fetal isovolumetric time intervals as a marker of abnormal cardiac function in fetal anemia from homozygous alpha thalassemia-1 disease. *Prenat Diagn*. 2017;37(10):1028-1032.
6. Tongsong T, Wanapirak C, Sirichotiyakul S, Chanprapaph P. Sonographic markers of hemoglobin Bart disease at midpregnancy. *J Ultrasound Med*. 2004;23(1):49-55.
7. Leung KY, Cheong KB, Lee CP, Chan V, Lam YH, Tang M. Ultrasonographic prediction of homozygous alpha0-thalassemia using placental thickness, fetal cardiothoracic ratio and middle cerebral artery Doppler: alone or in combination? *Ultrasound Obstet Gynecol*. 2010;35(2):149-154.
8. Srisupundit K, Piyamongkol W, Tongsong T. Identification of fetuses with hemoglobin Bart's disease using middle cerebral artery peak systolic velocity. *Ultrasound Obstet Gynecol*. 2009;33(6):694-697.
9. Harn-A-Morn P, Wanapirak C, Sirichotiyakul S, et al. Effectiveness of ultrasound algorithm in prenatal diagnosis of hemoglobin Bart's disease among pregnancies at risk. *Int J Gynaecol Obstet*. 2022;159(2):451-456.
10. Anuwutnavin S, Rangseechamrat P, Sompagdee N, Ruangvutilert P, Viboonchard S. Comparing three cardiothoracic ratio measurement techniques and creating multivariable scoring system to predict Bart's hydrops fetalis at 17-22 weeks' gestation. *Sci Rep*. 2024;14(1):8894.
11. Germanakis I, Matsui H, Gardiner HM. Myocardial strain abnormalities in fetal congenital heart disease assessed by speckle tracking echocardiography. *Fetal Diagn Ther*. 2012;32(1-2):123-130.
12. Miller TA, Puchalski MD, Weng C, Menon SC. Regional and global myocardial deformation of the fetal right ventricle in hypoplastic left heart syndrome. *Prenat Diagn*. 2012;32(10):949-953.
13. Truong UT, Sun HY, Tacy TA. Myocardial deformation in the fetal single ventricle. *J Am Soc Echocardiogr*. 2013;26(1):57-63.
14. DeVore GR, Polanco B, Satou G, Sklansky M. Two-dimensional speckle tracking of the fetal heart: a practical step-by-step approach for the fetal sonologist. *J Ultrasound Med*. 2016;35(8):1765-1781.
15. DeVore GR, Klas B, Satou G, Sklansky M. 24-segment sphericity index: a new technique to evaluate fetal cardiac diastolic shape. *Ultrasound Obstet Gynecol*. 2018;51(5):650-658.
16. Rychik J, Zeng S, Bebbington M, et al. Speckle tracking-derived myocardial tissue deformation imaging in twin-twin transfusion syndrome: differences in strain and strain rate between donor and recipient twins. *Fetal Diagn Ther*. 2012;32(1-2):131-137.
17. Miranda JO, Cerqueira RJ, Ramalho C, Areias JC, Henriques-Coelho T. Fetal cardiac function in maternal diabetes: a conventional and speckle-tracking echocardiographic study. *J Am Soc Echocardiogr*. 2018;31(3):333-341.
18. Tongsong T, Tongprasert F, Srisupundit K, Luewan S, Traisrisilp K. Ventricular diastolic function in normal fetuses and fetuses with Hb Bart's disease assessed by color M-mode propagation velocity using cardio-STIC-M (spatio-temporal image correlation M-mode). *Ultraschall Med*. 2016;37(5):492-496.
19. Thammavong K, Luewan S, Wanapirak C, Tongsong T. Ultrasound features of fetal anemia lessons from hemoglobin Bart disease. *J Ultrasound Med*. 2021;40(4):659-674.
20. Anuwutnavin S, Russameecharoen K, Ruangvutilert P, Viboonchard S, Sklansky M, DeVore GR. Assessment of the size and shape of the 4-chamber view and the right and left ventricles using fetal speckle tracking in normal fetuses at 17-24 gestational weeks. *Fetal Diagn Ther*. 2022;49(1-2):41-51.
21. Anuwutnavin S, Russameecharoen K, Ruangvutilert P, Viboonchard S, Sklansky M, DeVore GR. Reference ranges and development patterns of fetal myocardial function using speckle tracking echocardiography in healthy fetuses at 17 to 24 weeks of gestation. *Am J Perinatol*. 2024;41:1432-1444.
22. DeVore GR, Satou G, Sklansky M. Abnormal fetal findings associated with a global sphericity index of the 4-chamber view below the 5th centile. *J Ultrasound Med*. 2017;36(11):2309-2318.
23. DeVore GR, Klas B, Satou G, Sklansky M. Evaluation of fetal left ventricular size and function using speckle-tracking and the Simpson rule. *J Ultrasound Med*. 2019;38(5):1209-1221.
24. Tongsong T, Wanapirak C, Sirichotiyakul S, Piyamongkol W, Chanprapaph P. Fetal sonographic cardiothoracic ratio at midpregnancy as a predictor of Hb Bart disease. *J Ultrasound Med*. 1999;18(12):807-811.
25. Wanapirak C, Sirichotiyakul S, Luewan S, Srisupundit K, Tongprasert F, Tongsong T. Appearance of abnormal cardiothoracic ratio of fetuses with hemoglobin Bart's disease: life table analysis. *Ultraschall Med*. 2017;38(5):544-548.
26. Luewan S, Tongprasert F, Piyamongkol W, Wanapirak C, Tongsong T. Fetal liver length measurement at mid-pregnancy among fetuses at risk as a predictor of hemoglobin Bart's disease. *J Perinatol*. 2011;31(3):157-160.
27. Tongsong T, Wanapirak C, Sirichotiyakul S. Placental thickness at mid-pregnancy as a predictor of Hb Bart's disease. *Prenat Diagn*. 1999;19(11):1027-1030.
28. Thammavong K, Luewan S, Jatavan P, Tongsong T. Foetal haemodynamic response to anaemia. *ESC Heart Fail*. 2020;7(6):3473-3482.
29. Tongsong T, Wanapirak C, Piyamongkol W, et al. Fetal ventricular shortening fraction in hydrops fetalis. *Obstet Gynecol*. 2011;117(1):84-91.
30. Luewan S, Tongprasert F, Srisupundit K, Tongsong T. Inferior vena cava Doppler indices in fetuses with hemoglobin Bart's hydrops fetalis. *Prenat Diagn*. 2014;34(6):577-580.
31. Luewan S, Tongprasert F, Srisupundit K, Tongsong T. Fetal myocardial performance (Tei) index in fetal hemoglobin Bart's disease. *Ultraschall Med*. 2013;34(4):355-358.
32. Luewan S, Tongprasert F, Srisupundit K, Tongsong T. Fetal cardiac Doppler indices in fetuses with hemoglobin Bart's disease at 12-14weeks of gestation. *Int J Cardiol*. 2015;184:614-616.
33. Chao G, Zheng C, Meng D, et al. Tei index: the earliest detectable cardiac structural and functional abnormality detectable in Hb Bart's foetal edema. *Int J Cardiol*. 2009;134(3):e150-e154.
34. Srisupundit K, Luewan S, Tongsong T. Prenatal diagnosis of fetal heart failure. *Diagnostics (Basel)*. 2023;13(4):779.
35. Jatavan P, Chattipakorn N, Tongsong T. Fetal hemoglobin Bart's hydrops fetalis: pathophysiology, prenatal diagnosis and possibility of intrauterine treatment. *J Matern Fetal Neonatal Med*. 2018;31(7):946-957.
36. DeVore GR, Haxel C, Satou G, et al. Improved detection of coarctation of the aorta using speckle-tracking analysis of fetal heart on last examination prior to delivery. *Ultrasound Obstet Gynecol*. 2021;57(2):282-291.
37. DeVore GR, Cuneo B, Sklansky M, Satou G. Abnormalities of the width of the four-chamber view and the area, length, and width of the ventricles to identify fetuses at high-risk for D-transposition of the great arteries and tetralogy of fallot. *J Ultrasound Med*. 2023;42(3):637-646.

SUPPORTING INFORMATION ON THE INTERNET

The following supporting information may be found in the online version of this article:

Table S1 Parental demographic characteristics for fetuses with and those without hemoglobin (Hb) Bart's disease

Appendix S1 Individual probability for each of 29 non-hydropic fetuses with hemoglobin (Hb) Bart's disease and 77 unaffected controls

Appendix S2 Excel calculator for computation of probability of hemoglobin (Hb) Bart's disease, with example calculations. The tab labeled 'Sample Calculations' contains the equations for the mean and SD; these can be observed by placing the cursor over each of the measurements, which then displays the equation in the formula bar